Journal of Marine Research, 67, 273–303, 2009

Journal of
MARINE RESEARCH

Volume 67, Number 3

Mechanisms of variability in a convective basin

by Julie Deshayes[1,2,3], Fiammetta Straneo[1] and Michael A. Spall[1]

ABSTRACT

An idealized model for a convective basin is used to investigate the mechanisms of variability of the formation and export of dense water. In this model, which consists of two isopycnic layers, dense water formation is induced by surface buoyancy loss in the interior, which is at rest. Newly formed dense water is transmitted to the surrounding boundary current through parameterized eddy fluxes. Variability in the formation and export of dense water is due to changes in the two main drivers: variations in the surface buoyancy fluxes and variations in the large-scale wind via a barotropic boundary current. Numerical integrations of the nonlinear model, with parameters and forcings corresponding to the Labrador Sea, show that the rate of dense water formation in the interior of the basin is strongly affected by changes in the buoyancy forcing, but not significantly affected by seasonal to interannual changes in the wind-driven barotropic boundary current. The basin tends to integrate the buoyancy forcing variability with a memory time scale set by eddies, which is decadal for the Labrador Sea. Variability in dense water export, on the contrary, is strongly affected by changes in the wind-driven barotropic boundary current but hardly affected by changes in buoyancy forcing. Indeed changes in the transport of dense water at the basin outflow are dominated by those at the basin inflow, which, in this model, are directly related to fluctuations in the wind-driven barotropic boundary current. These results, which are consistent with analytical solutions of the linear model, suggest that fluctuations in the surface buoyancy fluxes in the interior Labrador Sea have little impact on the interannual variability of the dense water transport by the Deep Western Boundary Current at the outflow of the Labrador Sea, which is dominated by fluctuations in the wind-driven North Atlantic subpolar gyre, but influence the formation and export of recently ventilated waters.

1. Department of Physical Oceanography, Woods Hole Oceanographic Institution, Woods Hole, Massachusetts, 02543, U.S.A.
2. Present address: Laboratoire de Physique des Océans, CNRS, LPO UMR 6523, 29280 Plouzané, France.
3. Corresponding author. ***email: deshayes@ifremer.fr***

1. Introduction

The oceanic meridional overturning circulation (MOC) contributes substantially to the energy balance of the present climate, in particular via a net heat transport from the equator poleward in the North Atlantic (hereafter noted PHT for poleward heat transport, Trenberth and Caron, 2001; Talley, 2003). The heat that is transported northward in the upper ocean is released to the atmosphere at mid to high latitude, in particular in the subpolar North Atlantic and the Nordic seas where convection occurs and dense water is formed. The MOC and the PHT appear to be sensitive to changes in the convective activity in the North Atlantic, as suggested by modeling studies based on AOGCMs (coupled Atmosphere and Ocean General Circulation Models, e.g., Hawkins and Sutton, 2007) as well as those of intermediate complexity (Mignot *et al.*, 2007). For example, freshwater hosing experiments, where the rate of dense water formation is reduced due to an input of less-dense freshwater that stabilizes the upper stratification, show a significant decrease of the MOC and the PHT (Stouffer *et al.*, 2006) and a considerable impact on the overall climate (e.g., Vellinga and Wood, 2002; Pohlmann *et al.*, 2006).

Nevertheless, at the present time, observations of the MOC and the PHT are insufficient to study whether and how they are related to dense water formation in the North Atlantic. The longest continuous estimate of the MOC strength comes from observations of the Deep Western Boundary Current (hereafter DWBC) in the subpolar North Atlantic, which is the major export pathway of dense water formed in the North Atlantic (Talley and McCartney, 1982) and hence contributes to the deep limb of the MOC. The transport of dense water by the DWBC showed very similar mean and variance in two 2-yr-long surveys 6 years apart, although convection had changed considerably during that period (Schott *et al.*, 2004). As changes in the transport of dense water by the DWBC are expected to be related to fluctuations in the strength of the MOC, this suggests that there is neither a simple nor a direct connection between the MOC and dense water formation on the interannual to decadal time scale. The relation between dense water transport by the DWBC and the MOC remains to be clarified, though.

Besides, there is growing evidence that changes in the MOC and PHT may be driven by wind, in the absence of changes in dense water formation. For example, modeling studies suggest that the wind-driven Ekman transport drives monthly to interannual variability of the MOC and of the PHT at mid-latitude (e.g., Eden and Willebrand, 2001; Jayne and Marotzke, 2001). Hence changes in the MOC and the PHT would result from changes in wind forcing as well as changes in buoyancy forcing via dense water formation. Recent theoretical studies clarify the interactions between the wind- and the buoyancy-forced MOC by using idealized box models representing the global ocean (McMynowski and Tziperman, 2006; Johnson *et al.*, 2007), but it remains unclear how both forcings interact in a convective basin, such as the Labrador Sea, i.e., on spatial scales 10^2 to 10^3 km.

In a convective basin, dense water formation is induced by fluxes of buoyancy, predominantly heat, from the ocean to atmosphere. The net annual heat loss is balanced by the convergence of heat by the oceanic circulation, via the surrounding boundary current

(Spall, 2004). Wind forcing also acts over the convective basin and may affect dense water formation and export through various processes: (1) buoyancy forcing through the local impact of wind stress on the latent heat fluxes, (2) Ekman transport of heat and freshwater in the upper ocean, (3) vorticity input by the wind affecting the density distribution, which may precondition (or not) the water column and favor (or inhibit) buoyancy-driven convection (Marshall and Schott, 1999) and (4) circulation around the convective basin that determines the amount of heat entering the basin. In this study, we are only addressing a subset (4) of the possible effect of wind over a convective basin. By geostrophy, the large-scale cyclonic circulation around a convective basin is sustained by buoyancy forcing and dense water formation in the interior of the basin, but it is also driven by large-scale wind forcing. Similarly, variability of the boundary currents can be induced by changes in both wind and buoyancy forcings. However, hindcast simulations of the North Atlantic circulation suggest that variability induced by changes in the wind forcing over the subpolar gyre is the main driver of interannual variability of the boundary currents (Eden and Willebrand, 2001). Hence one question that we address in this paper: how do changes in the large scale circulation around a convective basin impact dense water formation and export ? It is important to note that we are not investigating other possible effects of wind forcing over a convective basin, hence this study should be considered as a first step toward understanding the more complex response of a convective basin to wind forcing.

In this idealized picture of a convective basin, another component has to be introduced to close the heat balance. The exchange of properties between the interior and the boundary current is achieved via turbulent transfers associated with baroclinic instabilities, which, in turn, are due to the density gradient between the interior and the boundary current (Spall, 2004). When adapted to the Labrador Sea, the conceptual model of Straneo (2006b), which employs a parameterization of these turbulent fluxes, reproduces seasonal and interannual fluctuations of the basin stratification and circulation that are similar to observations (Straneo, 2006a). This suggests that eddies play an essential role in convective basins such as the Labrador Sea that extends beyond their small spatial scale ($<$20 km) and their short lifetime (of the order of a few months), which is consistent with observations (Lilly *et al.*, 2003) and other modeling studies (Eden and Böning, 2002; Katsman *et al.*, 2004; Chanut *et al.*, 2008).

It is not straightforward to relate the mechanisms of variability in the convective basins of the North Atlantic, such as the Labrador Sea, to those of the large-scale MOC and PHT, as water masses that exit a convective basin are only partly exported to lower latitudes where they actually contribute to the global-scale MOC, the rest recirculating at high latitude. Nevertheless, we propose a first step toward understanding better the connection between the MOC, the PHT and dense water formation in the North Atlantic, by focusing on convective basins and investigating the respective influence of variability in buoyancy-driven convection and large-scale wind-driven circulation on the formation and export of dense water. Hence all physical discussions about the MOC and PHT hereafter are pertinent to convective basins alone. As eddies play an essential role in the heat balance of convective basins, an ensuing question is whether they influence variability on interannual to decadal time scales,

on which we focus. We use a conceptual model of a convective basin (Straneo, 2006b) and investigate its response to two external forcings: changes in buoyancy forcing and changes in wind forcing. The latter are simply represented as fluctuations of the barotropic circulation around the basin. The model formulation, outlined in Section 2, applies to any convective basin, but forcings (Section 3) and numerical simulations (Section 4) are for an idealized representation of the Labrador Sea. Analytical developments of a linear version of the model are presented in Section 5 to understand better the mechanisms of variability. The results are discussed in Section 6, taking into account a few of the model assumptions, and summarized in Section 7.

2. The model

We propose a simple model for a convective basin based on several assumptions, inspired from the Labrador Sea case, which are listed below:

- The circulation in a convective basin can be decomposed in two distinct regions: a steady interior, which is mostly horizontally homogeneous, and a surrounding boundary current, flowing along the topographic slopes (Straneo, 2006b). Hence there is an exchange but no net mass flux between the two regions. The model consists of these two regions, and the approximate location is indicated in Figure 1 (top) for the case of the Labrador Sea.
- As described in Straneo (2006b), the process of dense water formation in the Labrador Sea can be reproduced using two water masses: (1) light Irminger Current water, carried in by the boundary current, which provides heat to restratify the interior of the basin where (2) dense Labrador Sea water is formed. Freshwater inputs in the upper ocean, associated with precipitation, sea ice melting and river run-off, all contribute to restratifying the mixed layer after convection occurred, but they are negligible compared to the buoyancy fluxes associated with the lateral heat exchanges between the boundary current and the interior of the basin (Straneo, 2006a). To simplify, we do not represent variability in the upper ocean, above 200 m approximately. Similarly, the model does not contain water masses denser than those formed in the convective basin, such as overflow waters from the Nordic Seas that do not contribute to the formation and export of Labrador Sea water (Pickart and Spall, 2007). As a result, there are only two water masses represented in the model, of densities ρ_1 and ρ_2 ($\rho_2 > \rho_1$).
- In the interior of the convective basin, surface buoyancy forcing Q induces dense water formation. In the Labrador Sea, there is also dense water formation in the boundary current, related to local surface buoyancy fluxes (Pickart *et al*., 1997), but it is partly impeded by freshwater in the upper part of the water column. Hence the omission of Q over the boundary current in the model. The influence of this assumption on the model results is discussed in Section 6.
- Wind forcing has various impacts on a convective basin, several being listed in introduction. In this study, we only take into account the large-scale impact of wind forcing,

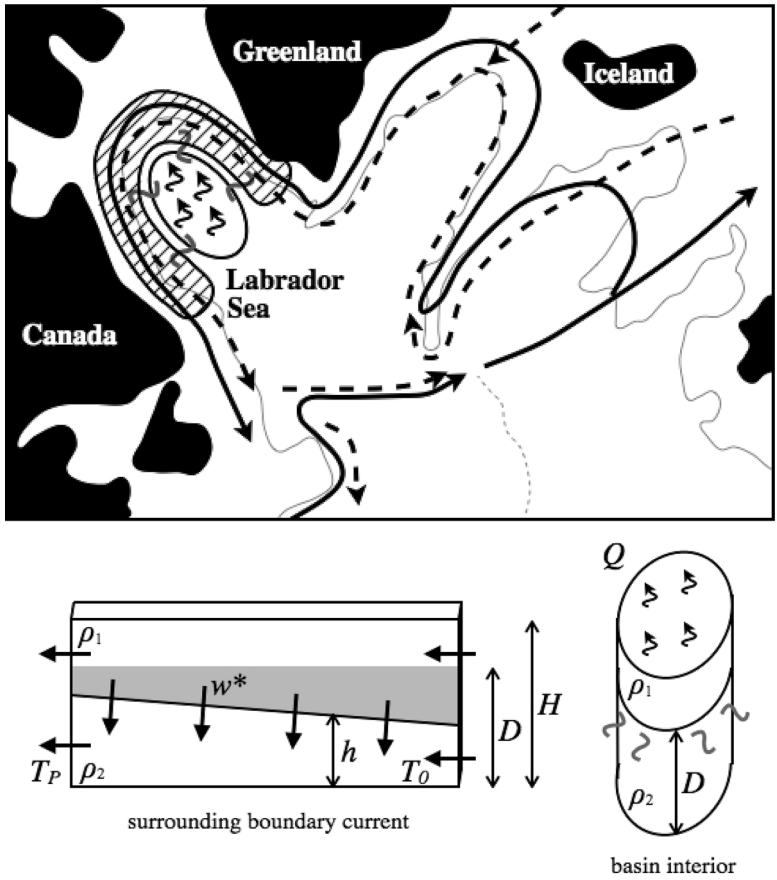

Figure 1. Schematic of the circulation in the North Atlantic (top, plain lines for warm water in the upper ocean, dashed lines for cold water at depth) and localization of the region of dense water formation in the central Labrador Sea (thin black line) and the surrounding boundary current (hatched area). The connection between the interior region, where dense water is induced by heat loss at the surface (black winding arrows), and the surrounding boundary current that exports the newly formed dense water, is primarily due to turbulent heat fluxes (gray winding lines). Bottom: schematic of the two regions of the conceptual model. Variables and parameters are defined in the text.

which is represented by a barotropic boundary current v_w. Note that assuming that the wind-forced circulation is barotropic, implies that wind forcing does not directly affect density structure in the interior of the basin. Nevertheless it contributes to the large-scale density gradient between the interior and the boundary current (i.e., the doming of isopycnals in the center of a convective basin) via advection of properties along the boundary current. In a practical manner, v_w is related to the large-scale wind stress curl via Sverdrup dynamics as any western boundary current.

Here is how the model works. Surface buoyancy forcing Q induces dense water formation in the interior of the basin, i.e., an increase in dense water thickness D (Fig. 1, bottom). The latter creates a density gradient between the interior and the surrounding boundary current, where dense water thickness h is smaller (gray shading). This horizontal density gradient drives a baroclinic component to the cyclonic boundary current. As the horizontal density gradient is unstable, it generates turbulent heat fluxes, parameterized in the model, and diapycnal mixing w^* within the boundary current (as there are no mass fluxes between the two regions). This finally leads to an increase in dense water thickness in the boundary current, while dense water thickness in the interior decreases asymptotically to h_0, the thickness of dense water at the boundary current inflow. Stratification in the boundary current is also influenced by the advection of properties within the boundary current, which depends on the inflow condition h_0, the barotropic wind-forced boundary current v_w, and the horizontal density gradient between the interior and the boundary current via thermal wind. Finally, dense water export T_P depends on w^* and the inflowing transport of dense water T_0.

Bearing in mind the questions that we address in this paper, namely the respective influence of a wind-driven barotropic boundary current and buoyancy-driven convection on dense water formation and export in a convective basin, we will be discussing variability in dense water thickness in the interior of the basin D, the rate of dense water formation w^* and the transport of dense water at the outflow of the basin T_P. It is important to note that T_P represents the transport of all dense water at the boundary current outflow, i.e., a mixture of recently formed dense water, subsequent to buoyancy forcing in the interior of the basin, and dense water that entered the basin at the boundary current inflow via T_0.

We briefly describe the equations governing the model. The reader is referred to Straneo (2006b) for more details on the analytical development of these equations. In the interior of the basin, where there is no mean flow, the changes in dense water volume are induced by surface buoyancy fluxes, Q, and lateral turbulent fluxes with the surrounding boundary current, noted $\overline{u'\rho'}$. Given the assumption that the interior is homogeneous, this writes

$$\Delta\rho\frac{dD}{dt} + \frac{1}{A}\int\int\overline{u'\rho'}dzdl = \frac{\rho_0}{g}Q \tag{1}$$

where $\Delta\rho = \rho_2 - \rho_1$, A is the interior area, g is gravity, ρ_0 is a density reference and l is the along-boundary coordinate, ranging from 0 at the inflow to P at the ouflow. The lateral turbulent fluxes are generated by the unstable density gradient between the interior and the boundary current. Following Spall (2004) and Straneo (2006b), they are chosen to depend on the density gradient between the interior and the surrounding boundary current:

$$\overline{u'\rho'} = c\Delta\rho(z)v_{bcl} \tag{2}$$

where c is a nondimensional parameter representing the efficiency of the eddies depending on the topographic slope (Spall, 2004), $\Delta\rho(z)$ is the density difference between the interior

and the boundary current, and v_{bcl} is the baroclinic velocity of the boundary current. As the latter is proportional, by geostrophy, to the density difference between the interior and the boundary current, $\overline{u'\rho'}$ is effectively proportional to $(\Delta\rho(z))^2$.

In the boundary current, changes in the thickness of the dense layer are due to the lateral turbulent fluxes and the non-divergence of the circulation:

$$L\Delta\rho\frac{\partial h}{\partial t} + L\Delta\rho\frac{\partial}{\partial l}(vh) = \int_H \overline{u'\rho'}\,dz \tag{3}$$

where L is the width of the boundary current and v is the velocity in the dense layer of the boundary current. Note that the total depth in the basin H is assumed to be constant, i.e., changes in the sea level are assumed negligible compared to the changes in isopycnal depth.

The velocity in the boundary current is decomposed into the baroclinic component v_{bcl}, implied by geostrophy as proportional to the density gradient between the interior and the boundary current, and the barotropic component v_{btp}. In the lower layer, it writes:

$$v(t,l) = v_{btp}(t) - v_{bcl}(t,l)\frac{H - h(t,l)}{H} \tag{4}$$

Note that because of mass conservation and the assumption that H is constant, the barotropic boundary current is a function of time only: $\frac{\partial v_{btp}}{\partial l} = 0$. At the inflow, where $h(t,0) = h_0$, the boundary current transports dense water formed in the interior Labrador Sea that recirculated within the Irminger Sea (e.g., Talley and McCartney, 1982; Lavender *et al.*, 2000) as well as dense water formed upstream, for example in the Irminger Sea (Pickart *et al.*, 2003; Falina *et al.*, 2007). Because little is known about the time scale of such a recirculation nor the fraction of inflowing dense water that was formed upstream of the Labrador Sea, we assume that the inflowing transport of dense water in the model is not directly related to the density distribution inside the basin (see Straneo, 2006b, for a discussion about this assumption). Hence at the inflow, the velocity of the lower layer is

$$v(t,0) = v_w(t)$$

while the velocity of the upper layer is $v_w(t) + v_{bcl}(t,0)$. The inflowing transport of dense water is then equal to

$$T_0(t) = h_0 \times L \times v_w(t)$$

where h_0, the thickness of dense water at the inflow, is assumed to be constant in time. Hence the inflowing transport of dense water is directly proportional to the barotropic current, v_w. As a result, in the following discussions, variations in wind forcing are mentioned as fluctuations of v_w, the wind-driven barotropic boundary current, or T_0, the inflowing transport of dense water, interchangeably.

From the inflow conditions, we can derive an expression for the barotropic velocity:

$$v_{btp}(t) = v_w(t) + v_{bcl}(t,0)\frac{H - h_0}{H}$$

which, introduced in (4), and assuming that $v_{bcl}(t,l) = v^* \frac{D(t)-h(t,l)}{H}$ as in Straneo (2006b), yields the following expression for the velocity in the lower layer of the boundary current:

$$v(t,l) = v_w(t) + v^* \frac{D(t)-h_0}{H}\frac{H-h_0}{H} - v^* \frac{D(t)-h(t,l)}{H}\frac{H-h(t,l)}{H} \tag{5}$$

where $v^* = \frac{2g'H}{f_0 L}$, g' is the reduced density and f_0 the Coriolis parameter (assumed to be constant).

Finally, introducing (2) in (1) and (3), we obtain the two model equations:

$$\frac{d}{dt}D(t) + \frac{2cg'}{Af_0L}\int_0^P (D(t)-h(t,l))^2 dl = \frac{Q(t)}{g'} \tag{6}$$

$$\frac{\partial}{\partial t}h(t,l) + \frac{\partial}{\partial l}\{v(t,l)h(t,l)\} = \frac{2cg'}{f_0L^2}(D(t)-h(t,l))^2 \tag{7}$$

The model outputs that we are interested in are the thickness of dense water in the interior of the basin $D(t)$, the dense water export $T_P(t) = h(t, P) \times L \times v(t, P)$ (which consists of recently formed dense water and dense water that entered the boundary current at the inflow) and the net diapycnal mixing within the boundary current $w^*(t) = T_P(t) - T_0(t)$. The latter represents the conversion of light to dense water in the boundary current, hence is proportional to the net buoyancy transport associated with the circulation, that is to say the heat transport in our simple model where salinity is not taken into account. Hence w^* can be interpreted as the PHT for the convective basin. In the context of the Labrador Sea, T_P represents the dense water transport at the exit of the Labrador Sea, e.g. the DWBC before it encounters the North Atlantic Current and splits into a recirculation branch of the subpolar gyre and a southward flow along the western boundary (see discussion in Section 6). It is not simple to relate these quantities to the large-scale MOC, because the latter can be defined in different ways. When considering the MOC as the zonal average of the meridional circulation in *density* coordinates, w^* would be the intensity of the MOC. However, this is not true when considering the MOC in *depth* coordinates. Moreover, hindcast simulations suggest that the MOC correlates well with the transport of dense water by the DWBC in the southern Labrador Sea (Böning *et al.*, 2006, Deshayes and Frankignoul, 2008), that is to say with T_P in our simple model. To avoid confusion in the rest of the paper, we discuss our results in terms of dense water transport by the DWBC and PHT rather than MOC.

We first present solutions of the nonlinear model (6) and (7) solved numerically, using a time stepping decomposition of the coupling. The time step used is 1 hour, but the outputs are monthly averages. Spatial step for the along-boundary coordinate is 5 km. Laplacian diffusivity has been added to (7) to dampen numerical instabilities in the divergence calculation, which is solved by a centered second-order scheme. The model has been spun up from rest for 25 years. The parameters used to represent the Labrador Sea are the same as in Straneo (2006b): $R = 230$ km (radius of the basin interior), $H = 1500$ m, $g' = 4.8\ 10^{-4}$ m s^{-2} (reduced gravity), $f_0 = 10^{-4}$ s^{-1}, $L = 100$ km and $c = 0.03$. Characteristics of the forcings are described below.

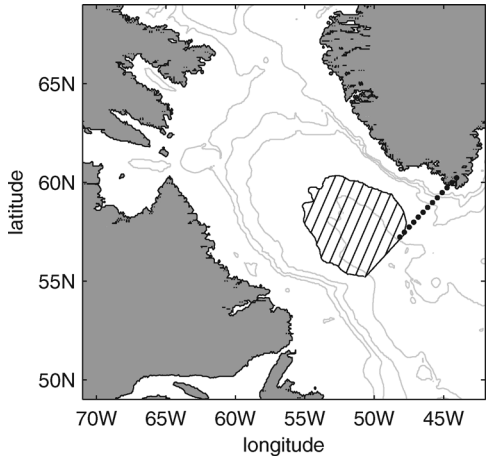

Figure 2. Topography of the Labrador Sea (thin gray lines indicate bathymetry contours 500 m, 1500 m, 2500 m and 3500 m, from ETOPO5 data). Stripes locate the closed area used to integrate the heat fluxes in the interior of the basin, while black dots indicate the location of WGC section.

3. Forcings for the Labrador Sea case

Straneo (2006a) discussed the large uncertainty involved in the estimates of the surface heat fluxes in the Labrador Sea. As in Straneo (2006a) and (2006b) we use the NCEP-NCAR reanalysis data (Kalnay *et al.*, 1996) recomputed for the period 1948–2000 (K. Moore, 2001, personal communication) to correct the overestimated net heat loss under extreme wintertime conditions (Renfrew *et al.*, 2002). The total heat fluxes (positive from the ocean to atmosphere) are integrated over the interior of the Labrador Sea, as defined by the 3300 m isobath and closed by a straight line at the southeastern end (Fig. 2). Heat fluxes from the interior of the Labrador Sea to the atmosphere exhibit strong seasonal variability (Fig. 3 top, black line). The cumulative heat lost by the ocean since May is negative, meaning that the ocean is gaining heat, until January when it changes sign and becomes positive (Fig. 3, bottom left, plain line). The net heat lost by the ocean, which leads to the formation of new dense water masses, occurs in January, February, March and April and amounts to 0.9 GJm^{-2} on average over the reanalysis period. This is equivalent to applying constant heat fluxes of 87 Wm^{-2} from January to April. We chose to only represent the seasonal fluctuations of the hydrography and circulation that are related to dense water formation, consistent with our 2-layer model that does not consider seasonal thermocline. Hence the heat fluxes applied to the model are 0 from May to December and account for the net yearly heat loss from January to April (Fig. 3, bottom left, dashed line).

There is pronounced variability in the yearly net heat loss over the interior of the Labrador Sea (Fig. 3 top, gray line). Standard deviation of the yearly data is 0.44 GJm^{-2} and the power spectrum density suggests that the time series behaves as a white noise (Fig. 3, bottom right). For the interannual simulations, we create a 250-yr-long time series of the yearly net heat

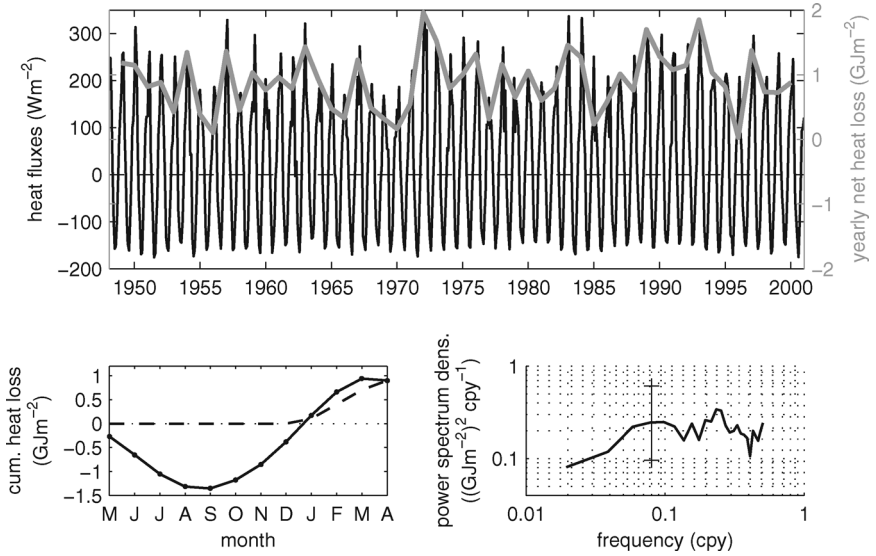

Figure 3. Heat fluxes in the interior of the Labrador Sea from 1948 to 2001 from monthly NCEP-NCAR reanalyses (top, black line reading with left-hand axis, hereafter convention is positive heat fluxes from the ocean to atmosphere) and yearly net heat loss (gray line reading with right-hand axis). Oceanic heat loss cumulated from May to April from observations (bottom left, plain line) and idealized to force the model (dashed line). Spectrum of the net yearly heat loss from 1948 to 2000 (bottom right), calculated using the multitaper method using five windows, the 95% confidence level is given by the vertical line.

loss with the same spectral characteristics as in the NCEP-NCAR data, by multiplying the seasonal heat fluxes by a random time series normalized so that the standard deviation of the yearly data equals the estimate from NCEP-NCAR data.

Boundary condition of the model at the inflow requires us to specify h_0, the thickness of dense water inflowing to the basin, and v_w, the wind-forced barotropic velocity. Observations of the West Greenland Current, defined here as the northwestward current along the southwestern coast of Greenland, describe the mean hydrography (Cuny *et al.*, 2002; Pickart and Spall, 2007) and suggest changes in the amount of warm water that enters the Labrador Sea (Myers *et al.*, 2007). Nevertheless, they remain insufficient to determine the amplitude and time scale of those fluctuations. Hence, in this study, it is assumed that $h_0 = 700$ m (from Straneo, 2006b, her Fig. 5) and that its value is constant in time (see discussion in Section 6). We instead consider fluctuations in v_w and their impact on dense water formation and export. In our model, v_w is a barotropic component of the boundary current, hence of the West Greenland Current. Again, observations are insufficient to estimate seasonal and interannual fluctuations of the strength of the currents, hence we use a hindcast simulation of the North Atlantic from 1953 to 2003 (Deshayes *et al.*, 2007). Figure 4 shows the simulated circulation at the southern tip of Greenland (see location of

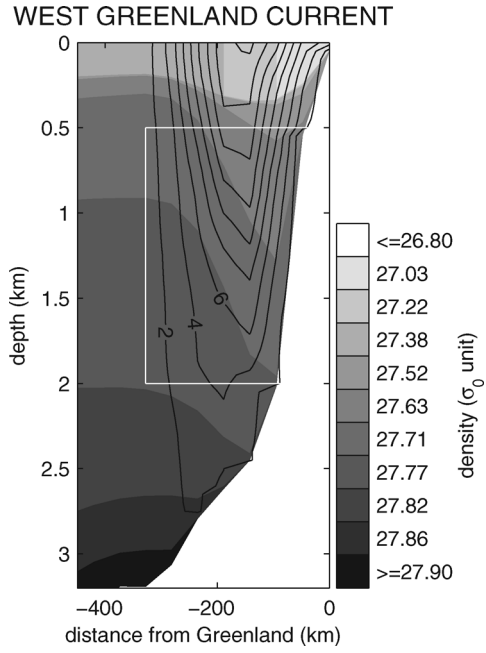

Figure 4. Mean West Greenland Current from 1953 to 2003: density (gray shading) and northwestward current across the section (black contours, in cm s^{-1}) from a hind-cast simulation of the circulation in the North Atlantic (Deshayes *et al*., 2007). White lines indicate the area where the transport is integrated.

the section in Fig. 2) on average from 1953 to 2003. The isopycnals that correspond to Irminger Current water and Labrador Sea water ($\sigma_0 = 27.63 - 27.77$ kg m^{-3}) are found from 500 m to 2000 m depth approximately; hence, we calculate the net transport within that depth interval, from the coast to about 300 km (Fig. 5 top, black line). Note that the characteristics of the transport variability do not depend on the selected depth interval. The net transport reaches 23 Sv on average, which corresponds to barotropic velocities of the order of 15 cm s^{-1}, consistent with observations (Pickart and Spall, 2007, their Fig. 6). The transport is maximum in winter, from January to March, and minimum and almost constant the rest of the year (Fig. 5, bottom left, plain line). To simplify, we assume that v_w is the total barotropic velocity at the inflow of our simple model, hence in our simulations of the Labrador Sea, v_w has similar seasonal fluctuations and is maximum 1 month before the heat fluxes peak (Fig. 5, bottom left, dashed line).

From the GCM hindcast simulation, the standard deviation of transport in the West Greenland Current, calculated from yearly averages as above (i.e., from 500 m to 2000 m and from the coast to about 300 km, see white line in Fig. 4) is 3 Sv. Estimates of that transport (integrated over the same area) from directly measured velocities in summer 1995 and 1996 are 29 Sv and 26 Sv respectively (Hall and Torres, 2008, pers. comm., see also Hall

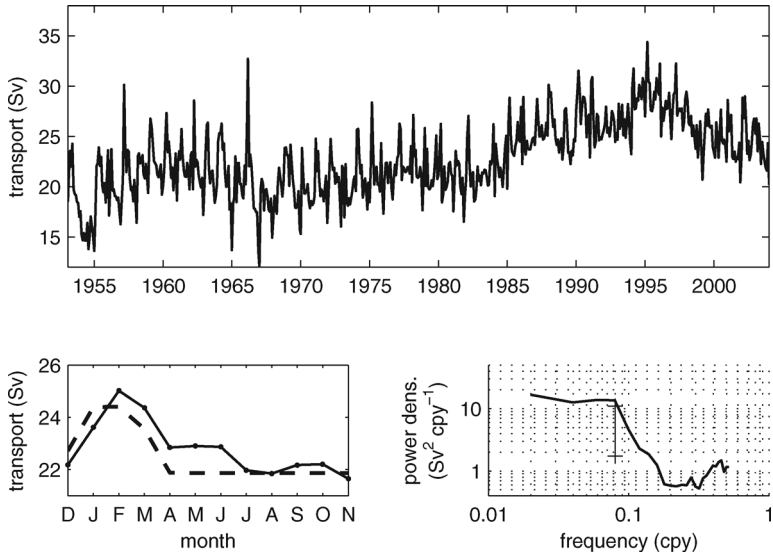

Figure 5. Transport in the West Greenland Current (top, black line), mean seasonal cycle (bottom left, plain line) and idealized seasonal cycle used to force the model (dashed line). Spectrum of the yearly West Greenland Current transport (bottom right), calculated using the multitaper method using five windows, the 95% confidence level is given by the vertical line.

and Torres, 2008), which somewhat validates the order of magnitude of the West Greenland Current transport variability in the GCM simulation. Standard deviation reduces to 2 Sv if the time series is linearly detrended. Indeed, the transport increased from the mid-1970's to the mid-1990's and then decreased, which projects on an increasing trend. In a coherent manner, the power spectrum density of the transport shows enhanced variability at decadal and longer periods (Fig. 5, bottom right). This simulated low-frequency variability reflects the subpolar gyre variability (Deshayes and Frankignoul, 2008), which is in part induced by wind variability over the North Atlantic. We note that the objective of this paper is not to clarify the mechanisms of adjustment of the subpolar gyre to wind forcing over the North Atlantic. Rather, in the perspective of simplying the problem, we assume that the West Greenland Current transport behaves as white noise and generate a random 250-yr-long time series to modulate the seasonal fluctuations of v_w in the model. For the Labrador Sea simulation (noted LABSEA in the following, see Table 1 for a list of all simulations), the standard deviation of the transport of dense water at the inflow is taken to be equal to 2.1 Sv.

4. Numerical experiments

The objective of the paper is to understand the response of a convective basin's MOC related quantities (namely dense water formation and export) to variable buoyancy forcing

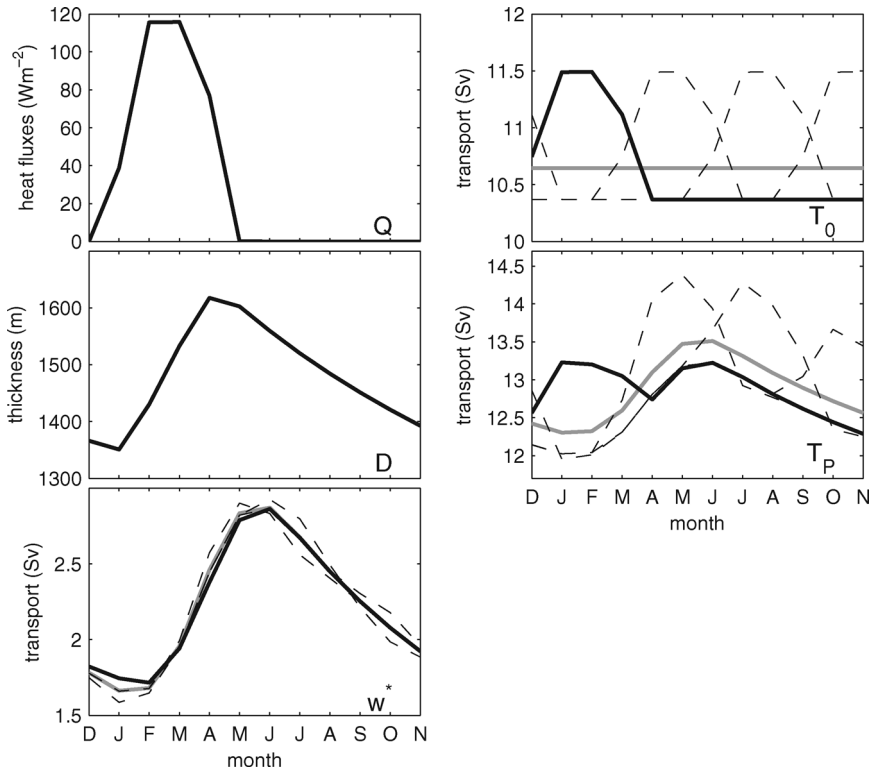

Figure 6. Seasonal cycle of model forcings (Q in and T_0, top panels) and outputs (D, T_P and w^*) for experiments STRANEO (T_0 is constant, gray lines) and SEASON (T_0 is seasonal and leads Q by 1 month, plain lines). Thin dashed lines represent sensitivity experiments when T_0 has seasonal modulation but leads Q by 4, 7 and 10 months.

on the surface and to a variable barotropic boundary current at the inflow. We first use numerical simulations with seasonal forcings only, then introduce interannual changes in both forcings. Note that we do not allow feedbacks from the convective basin response to the forcings.

Table 1. Parameters of the experiments: seasonal cycle of the surface buoyancy fluxes Q (Q seas.); standard deviation of the yearly net heat loss in the basin interior ($std(Q)$ in GJm^{-2}); seasonal cycle of the transport of dense water into the basin (T_0 seas.); standard deviation of the yearly averages ($std(T_0)$ in Sv) and r' (dimensionless) calculated from (15).

	Q seas.	$std(Q)$	T_0 seas.	$std(T_0)$	r'
STRANEO	yes	0	no	0	–
SEASON	yes	0	yes	0	–
LINEAR	yes	0	no	0	–
HEAT	yes	0.44	yes	0	∞
HEAT+BBC	yes	0.44	yes	0.7	5.4
LABSEA	yes	0.44	yes	2.1	0.61

The first set of numerical simulations use seasonal forcings only. A reference simulation, called STRANEO, is run with seasonal heat flux forcing and constant barotropic boundary current forcing, and yields the same results as discussed by Straneo (2006b): D peaks in April and slowly decreases due to the turbulent exchanges with the boundary current (Fig. 6, gray line). Note that for the chosen set of parameters and forcings, D may be larger than H, which is not critical but means that the whole interior is filled with dense water. T_P is maximum in June, similarly to w^*. When seasonal changes in T_0 are added via v_w (experiment SEASON), T_P is linearly modulated with no phase lag, while D and w^* are hardly affected (thick black lines). We computed additional experiments with different lags between Q and T_0 (thin dashed lines) that confirm that the circulation anomalies due to seasonal changes in buoyancy and barotropic boundary current forcing linearly superimpose.

These preliminary experiments suggest that the buoyancy-driven dense water formation is not affected by seasonal changes in the barotropic boundary current forcing. This result is not inconsistent with earlier findings in Straneo (2006b) who found that changes in the barotropic boundary current on long time scales affect dense water formation, as a larger v_w would induce an increase in the heat advected by the boundary current and then transferred by the eddies to the interior of the basin, which would lead to a smaller volume of dense water in the interior (Straneo 2006b, her Fig. 10b). Note that $< v_w(t) >$ in experiment SEASON, where the angle brackets denote the expectation operator, is equal to v_w in STRANEO, suggesting that dense water formation in the interior only cares about the mean heat transport in the boundary current.

Interannual fluctuations are then introduced in the buoyancy forcing (experiment HEAT, Fig. 7 gray lines) as well as in the barotropic boundary current forcing (experiment LABSEA, black lines, only the first 50 yr of the 250-yr-long time series are shown). T_P is affected by interannual changes in the barotropic boundary current forcing, while D and w^* are not. Autocorrelation of D is the same in both experiments and is significant at 1-yr-lag (Fig. 8, top left, e^{-1} indicates the decorrelation time scale for an autoregressive process) suggesting that the interior basin has a memory on interannual time scales. T_P is also autocorrelated at 1-yr-lag in experiment HEAT, but the autocorrelation rapidly drops in experiment LABSEA, suggesting that the memory associated with dense water formation in the interior of the basin is overwhelmed by fluctuations of the barotropic boundary current forcing in the boundary current (Fig. 8, bottom left). Figure 8 also shows the correlation between the model outputs and forcings for the two experiments HEAT and LABSEA (right panels). The correlation of D with Q is the same in both experiments and is maximum at a few month lag but remains significant until D lags Q by about 2 yr, while the correlation with T_0 in experiment LABSEA is not significant. The correlation of T_P with Q is significant in experiment HEAT but much smaller in experiment LABSEA, where the correlation with the barotropic boundary current forcing peaks at 0-yr lag and explains as much as 80% of the variance. What this means is that it takes a couple years for dense water formation to adjust to interannual changes in buoyancy forcing, which can be seen as a memory of the

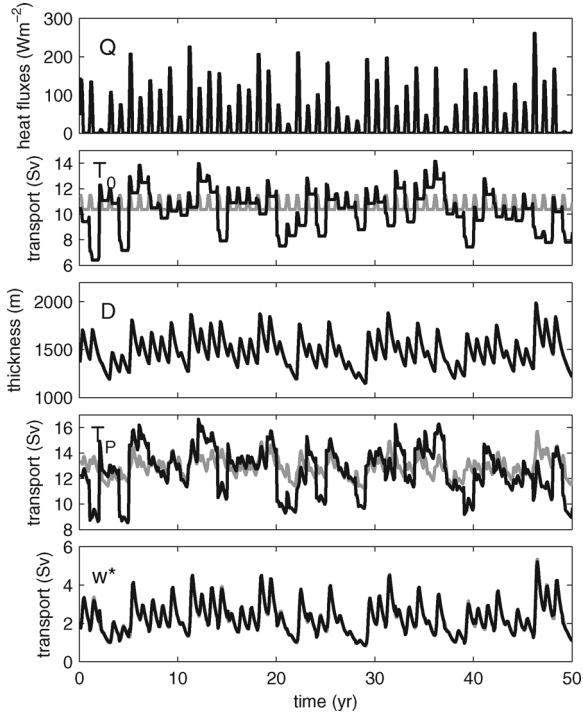

Figure 7. 50-yr time series of model forcings (Q and T_0, top panels) and outputs (D, T_P and w^*) for experiments HEAT (T_0 is seasonal but constant on the interannual time scale, gray lines) and LABSEA (both T_0 and Q vary on seasonal and interannual time scales, black lines).

basin interior. However this memory effect is not visible in the dense water export, since variability is dominated by changes in the inflowing transport of dense water, which, in turn, reflect changes in the barotropic boundary current forcing.

The interannual variability of the model outputs is further described by ensemble averages of multiple simulations based on the same initial conditions (the steady state from the spinup) but using different random time series for the interannual forcings. Convergence of the ensemble simulations is estimated from the ensemble average of the power spectrum densities $P_D(f_i)$ and $P_{T_P}(f_i)$ at high, intermediate and low frequencies for experiment LABSEA. The power spectrum density of a function F is defined as $P_F(f) =< \hat{F}(f)\hat{F}^*(f) >$, where the caret denotes the Fourier transform and the asterisk the complex conjugate. Figure 9 suggests that when using 100 simulations, the power spectrum density only slightly differs (of the order of 5%) from the ensemble average calculated over 200 simulations. Hence Figs. 10 and 11 show ensemble averages of $N = 100$ simulations.

The power spectrum density of D in experiment LABSEA is flat for periods longer than about 10 yr and significantly reduced for smaller periods, indicating that D has most

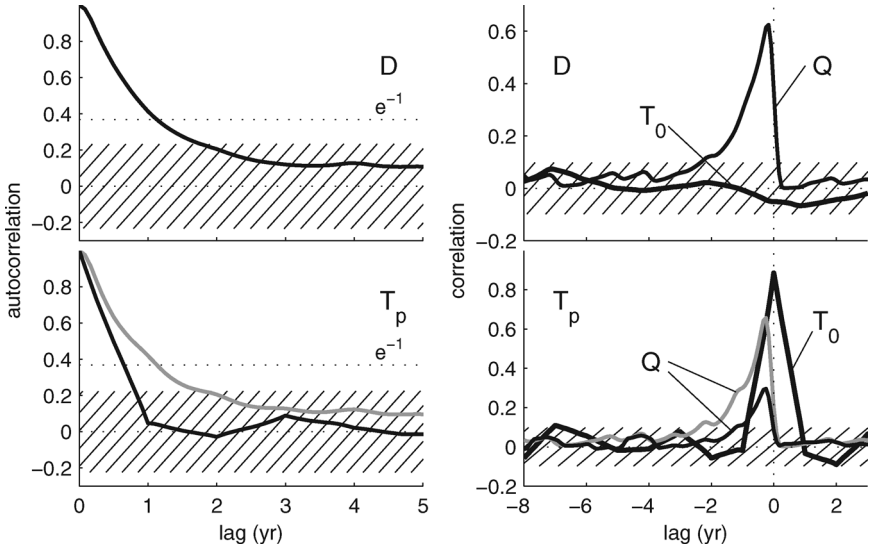

Figure 8. Autocorrelation of model outputs (left panels) and correlation with forcings (right panels) for experiments HEAT (T_0 is seasonal only, while Q is seasonal and interannual, gray lines) and LABSEA (Q and T_0 both vary on the seasonal and interannual time scales, black lines). Seasonal cycles and linear trends have been removed from all time series. Hatched area indicates where correlations are not significant (at 95% confidence). Forcings (Q and T_0) lead for negative lags.

variance a low frequency (Fig. 10, second panel, note that all power spectrum densities are calculated from yearly averages to focus on the interannual to decadal variability). At periods from 1 to 5 yr ($0.2 < f < 0.4$ cpy), P_D approximately varies as f^{-2}. Considering that both forcings are white noise, i.e., have flat spectra (top panel), this suggests that dense water formation in the interior behaves as a simple integrator, with a time scale of 7 yr ($f \approx 0.14$ cpy) determined by the change in slope in P_D. In experiment HEAT, where T_0 does not vary on the interannual time scale, P_D is exactly identical to that in LABSEA (not shown). Same is true for an additional experiment, called HEAT+BBC, where T_0 does vary on the interannual time scale but with a smaller variance than in LABSEA (see Table 1). This complements the previous results for the seasonal to interannual variability and confirms that changes in dense water formation in the interior basin are not influenced by fluctuations of the barotropic boundary current forcing in this idealized model.

The power spectrum density of T_P in experiment LABSEA shows no dependence on frequency (Fig. 10). However P_{T_P} strongly depends on the variability of T_0: in experiment HEAT, for which T_0 only varies on the seasonal time scale, P_{T_P} is almost constant and maximum for decadal to longer periods, while it is much reduced at higher frequency (Fig. 11, dashed line). In experiment HEAT+BBC, for which T_0 varies on the interannual time scale with a standard deviation three times as small as that in LABSEA, P_{T_P} is also maximum at decadal periods and significantly decreases at higher frequency, but not as

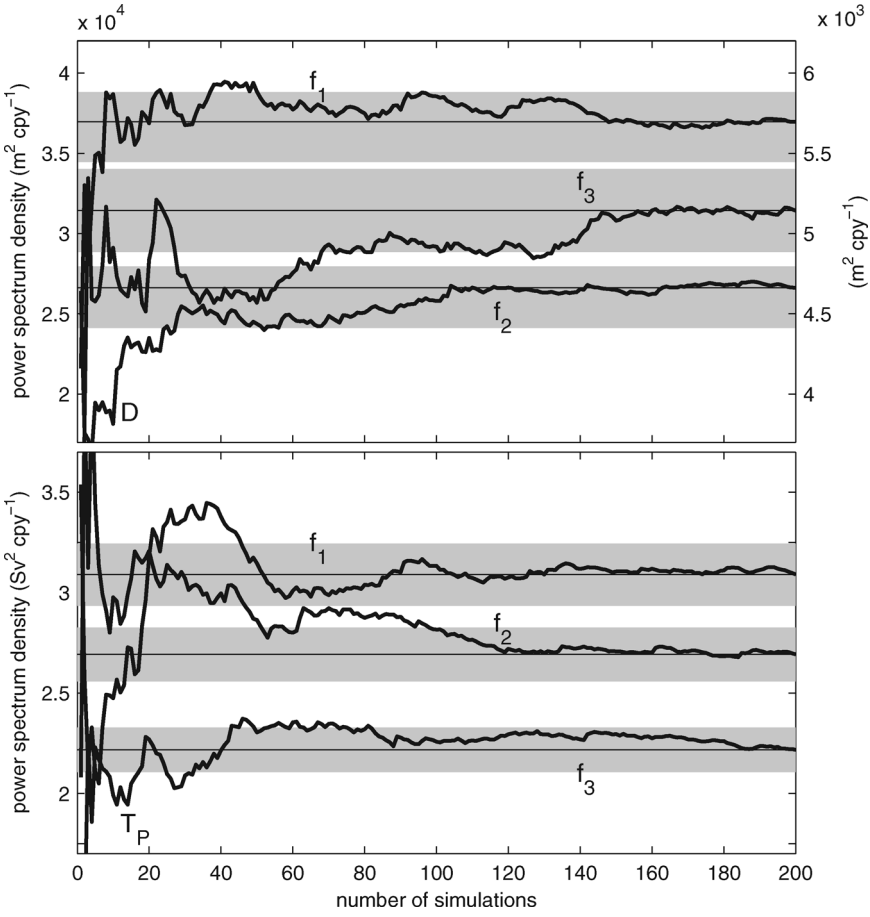

Figure 9. Ensemble average of the power spectrum density $< P_D(f_i) >$ (top) and $< P_{T_P}(f_i) >$ (bottom) for experiment LABSEA as a function of the number of simulations (thick lines), for three selected frequencies: $f_1 = 0.04$ cpy, $f_2 = 0.1$ cpy, $f_3 = 0.4$ cpy ($< P_D(f_3) >$ reads on the right-hand axis). Power spectrum densities are calculated with the multitaper method using five windows. Gray shading indicates, for each frequency, the 5% interval about the ensemble average (thin lines) calculated over 200 simulations.

much as in HEAT, suggesting a flattening of the spectrum at high frequency (dash-dotted line). Hence variability in barotropic boundary current forcing induces an increase in the variability of T_P, especially at interannual to decadal time scales, with respect to variability induced by changes in buoyancy forcing alone. The flattening of the spectrum at high frequency is consistent with the MOC spectrum in AOGCMs as shown by Deshayes and Frankignoul (2005) and Zhu *et al.* (2006). Indeed, in these studies, the MOC is defined in depth coordinates, hence its fluctuations are represented by changes in the dense water transport in the DWBC, that is to say T_P in our simple model.

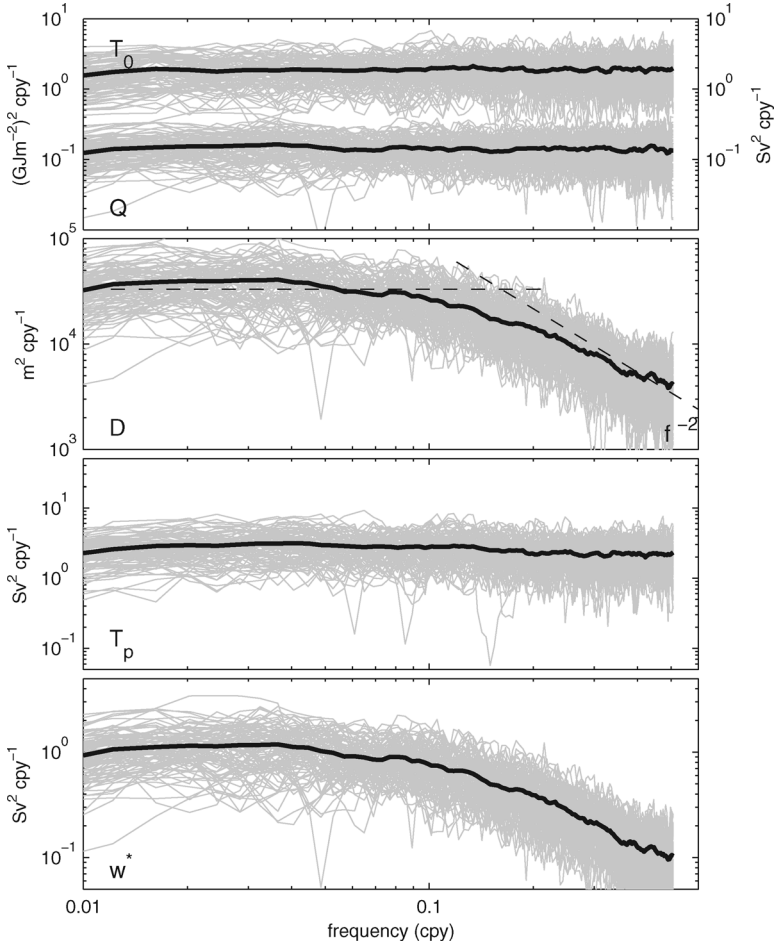

Figure 10. Ensemble simulations for experiment LABSEA: power spectrum of Q and T_0 (top, right-hand axis for T_0), D, T_P and w^* (bottom panels). Thin gray lines represent power spectra for individual experiments while thick black lines represent the ensemble averages. Spectra are calculated with the multitaper method using five windows. Dashed lines indicate constant and f^{-2} power laws for D spectra.

The power spectrum density of w^*, the diapycnal mixing within the boundary current, is very similar to P_D with maximum variance at decadal and longer periods (Fig. 10) and is similar in the three experiments (not shown). It is intriguing that the spectral shape of P_{T_P}, when there is interannual variability in barotropic boundary current forcing (experiments HEAT+BBC and LABSEA), differs from that of P_{w^*}. Indeed, w^* represents the conversion of light to dense water in the boundary current, hence the net buoyancy transport associated with the circulation. This suggests that variability of the dense water transport by the DWBC

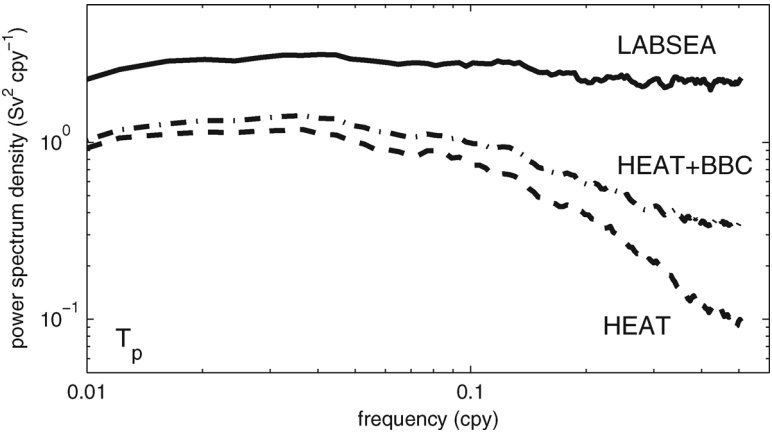

Figure 11. Ensemble average of the power spectrum density of T_P in experiments LABSEA (plain line), HEAT+BBC (dash-dotted line) and HEAT (dashed line). Spectra are calculated with the multitaper method using five windows.

at interannual time scales, which is primarily induced by changes in barotropic boundary current forcing, may not be associated with changes in the PHT.

Finally, numerical simulations suggest that the convective basin's MOC related quantities do not respond to buoyancy and barotropic boundary current forcing in the same fashion and exhibit different characteristics of variability: D is not affected by changes in barotropic boundary current forcing at seasonal and interannual timescale, and, together with w^*, they both have reduced variance at high frequency, while fluctuations of T_P are strongly correlated with changes in the barotropic boundary current at the basin inflow and has a variance that does not depend on frequency, except when the barotropic boundary current forcing is steady. Hence there seems to be different mechanisms of variability acting in the basin. We propose to identify them by looking at a linearized version of the model, which can be partly solved analytically.

5. Linear model

In order to identify better the mechanisms of variability that influence the model outputs, we come back to the equations of the model (6) and (7), which we simplify further by neglecting the nonlinearities. Details on the linearization of the model are given in the Appendix. Linearization assumes two hypotheses:

$$\gamma = \frac{v^*(D(t) - h_0)/H}{v_w + v^* h_0 (D(t) + H - 2h_0)/H^2} \times \frac{cP}{L} << 1 \tag{8}$$

and

$$\frac{AQ(t)}{g' L v_w(t) h_0} << 1. \tag{9}$$

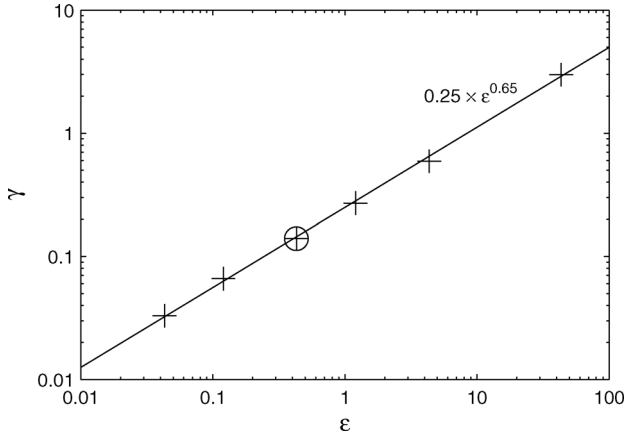

Figure 12. Parameter γ (8) as a function of ϵ for experiments LINEAR (crosses, both parameters are dimensionless). Black line represents $0.25 \times \epsilon^{0.65}$ function. LABSEA experiment, for which $\epsilon = 0.43$, is represented by a circle.

As mentioned in Straneo (2006b), γ is the product of two terms, both potentially small: the first is the ratio of the baroclinic velocity at inflow to the effective advective velocity for the dense layer thickness[4] at inflow; the second, noted $\epsilon = cP/L$, is a measure of the eddy efficiency (Spall, 2004, the larger ϵ, the larger portion of the heat transported by the boundary current is transferred by the eddies to the interior of the basin). The second hypothesis (9) assumes that the rate of dense water formation in the basin interior is small compared to the transport of dense water at the boundary current inflow. As noted in Straneo (2006b), it is satisfied when v_w is large. In other words, nonlinearities appear when barotropic boundary current forcing is weak. For the chosen set of parameters and forcings,

$$\gamma = 0.14 \text{ and } \frac{A < Q(t) >}{g'L < v_w(t) > h_0} = 0.21.$$

Hence the Labrador Sea is in the model's linear regime.

Because the following analytical developments strongly rely on the hypothesis that the model can be linearized for the Labrador Sea case, we estimated the range in parameters that corresponds to the linear case. As in Straneo (2006b), we consider γ as a measure of the non-linearities of the model and ran several simulations (experiment LINEAR) with Q seasonal and T_0 constant with different values of $\epsilon = cP/L$. Each simulation has been integrated for 10 yr after spinup, and $< D(t) >$ was calculated once the model had reached a steady state again. Figure 12 shows that γ approximately follows $0.25 \times \epsilon^{0.65}$, hence $\gamma > 1$

4. When writing the left hand side of (7) as the advection of dense layer thickness, it appears that the effective advective velocity is the sum of the velocity in the lower layer $v(t, l)$ plus a second term due to changes in the velocity in the lower layer $\frac{\partial v(t,l)}{\partial l}$, ultimately related to the changes in dense layer thickness $\frac{\partial h(t,l)}{\partial l}$ to satisfy mass conservation (Straneo, 2006b).

when $\epsilon > 10$. In the absence of wind-driven barotropic boundary current and if $\epsilon > 1$, the heat carried by the buoyancy-driven boundary current is entirely fluxed to the interior of the basin before the boundary current has extended around the basin (Spall, 2004). It is difficult to determine ϵ accurately for the Labrador Sea, but estimates range from 0.1 (Spall, 2004), 0.2 (Pickart and Spall, 2007) to 0.43 (Straneo, 2006b and in this study, indicated by the circle in Fig. 12). As a result, the range of parameters where non-linearities are negligible is fairly wide and linearization is a valid assumption for the Labrador Sea.

Assuming that the equations can be linearized (see appendix for some details about the linearization of the equations) and considering changes on interannual and longer time scales (which allows the boundary current to adjust to changes in the interior of the basin, see appendix), equation (7) has a unique solution:

$$h(t,l) = h_0 + \frac{1}{2}(D(t) - h_0)\left(1 - e^{\frac{-2\gamma l}{P}}\right). \tag{10}$$

Introducing (10) into (6) writes

$$\frac{d}{dt}D(t) + \frac{2cg'}{Af_0L}\int_0^P e^{-\frac{2\gamma l}{P}} dl\,(D(t) - h_0)^2 = \frac{Q(t)}{g'}$$

We now assume that anomalies $D'(t) = D(t) - < D(t) >$ and $Q'(t) = Q(t) - < Q(t) >$ are small compared to averages $< D(t) >$ and $< Q(t) >$ respectively, which finally gives

$$\frac{d}{dt}D'(t) + \Lambda^{-1}D'(t) = \frac{Q'(t)}{g'} \tag{11}$$

$$\text{with } \Lambda = \frac{A}{2 < v_{bcl}(t,0) > L\epsilon} \tag{12}$$

where $v_{bcl}(t,0)$ is the baroclinic velocity at the inflow. This suggests that dense water in the interior adjusts to fluctuations of the buoyancy forcing on time scale Λ. The latter can be seen as the eddy flushing time: it is proportional to the size of the basin interior, and inversely proportional to the mean baroclinic velocity at inflow, to the width of the boundary current and to the eddies efficiency. Note that Λ does not depend on v_w, although v_w has to be large enough to satisfy (9).

The time scale Λ plays a major role for the interannual variability of D. Introducing Fourier transforms $[D'(t), Q'(t)] = \int_{-\infty}^{+\infty}[\hat{D}(f), \hat{Q}(f)]e^{i2\pi ft}df$ in (11) yields

$$\hat{D}(f) = \frac{\hat{Q}(f)}{g'}\frac{1}{i2\pi f + \Lambda^{-1}}$$

hence the power spectrum density of $D(t)$ is

$$P_D(f) = \frac{P_Q(f)}{g'^2}\frac{1}{\Lambda^{-2} + (2\pi f)^2}.$$

This suggests that if P_Q does not depend on frequency (flat spectrum), P_D behaves as f^{-2} at high frequencies and flattens for frequencies $f < (\Lambda \times 2\pi)^{-1}$ cpy, consistent with the numerical experiments (Fig. 10). For the chosen set of parameters, $\Lambda^{-1} = 0.17$ cpy, which corresponds to the frequency at which the two spectral slopes of P_D cross. Finally, D can be considered as an integrator of the surface buoyancy flux variability with a characteristic time scale Λ that notably depends on the eddy efficiency. In the Labrador Sea case, this means that most variability of dense water formation is at the decadal and longer periods.

The dense water export can be analytically calculated when integrating (7) along the basin perimeter and using (6), which yields

$$T_P(t) - T_0(t) = \frac{AQ(t)}{g'} - A\frac{dD(t)}{dt} - L\frac{d}{dt}\int_0^P h(t,l)dl. \tag{13}$$

Introducing (10) and using primes to denote anomalies relative to the time averages as above, this simplifies into:

$$T'_P(t) = T'_0(t) + \frac{AQ'(t)}{g'} - (A + \gamma PL)\frac{dD'(t)}{dt}$$

We simplify this expression further by introducing (11) and neglecting the terms proportional to γ. Using the Fourier transforms as described above, this gives the power spectrum density for $T_P(t)$:

$$P_{T_P}(f) = P_{T_0}(f) + \left(\frac{A}{g'}\right)^2 \frac{\Lambda^{-2}}{\Lambda^{-2} + (2\pi f)^2} P_Q(f) \tag{14}$$

where we assumed that the correlation between the wind-driven barotropic boundary current and the surface buoyancy fluxes is negligible. Hence spectral characteristics of the dense water export result from the competition between (i) the direct influence of the barotropic boundary current, via P_{T_0} and (ii) the integration of the surface buoyancy fluxes variability P_Q with the time scale Λ. In experiment HEAT, for which $P_{T_0} = 0$, T_P acts as an integrator of Q and has a red spectrum, which resembles that of D, while in experiment LABSEA, P_{T_0} dominates the right hand side of (14) hence P_{T_P} is flat. In experiment HEAT+BBC, the fluctuations of the circulation driven by changes in buoyancy forcing are mostly important at decadal and lower frequency while those driven by fluctuations in the barotropic boundary current dominate at interannual frequencies.

Finally, we introduce the following ratio

$$r' = \frac{A^2 \int P_Q(f)df}{g'^2 \int P_{T_0}(f)df} = \frac{A^2 std(Q(t))^2}{g'^2 std(T_0(t))^2}$$

where $std(F)$ is the standard deviation of the yearly timeseries F, to identify, for a chosen set of forcings and parameters, which mechanism dominates the variability in dense water export (see Table 1 for the value of r' in the different experiments). If $r' < 1$, such as in the

Labrador Sea ($r' = 0.61$), the variability in dense water export is dominated by fluctuations in dense water import, ie in barotropic boundary current fluctuations in this simple model. If $r' > 1$, dense water export may also be influenced by changes in the buoyancy-driven dense water formation. Note that from (14), in the latter case, the more efficient the eddies, the smaller Λ and the larger the influence of the buoyancy-driven dense water formation on the dense water export. Even for cases with $r' < 1$, buoyancy-forcing remains important for the formation and export of recently ventilated waters.

6. Discussion

This study uses a conceptual model of a convective basin, which employs several assumptions. Here, our results are discussed in the light of these assumptions. We also discuss the implication of our results for the large-scale MOC and PHT as well as mid-latitude DWBC.

a. Eddy fluxes parameterization

Although eddies play a crucial role in convective basins such as the Labrador Sea, they are not resolved by the model. However their effect is parameterized as a turbulent transfer of heat between the interior of the basin and the boundary current (2). The parameterization used in the present study is the same as in Straneo (2006b), and is based on Spall (2004) who extends the general approach of Visbeck *et al.* (1996) and Spall and Chapman (1998) to instabilities over a sloping bottom. We note that there are other strategies to parameterize the heat fluxes due to baroclinic instabilities (two others are discussed in Visbeck *et al.*, 1997), but the results of Spall (2004) suggest that the downgradient parameterization (2) is appropriate for the instabilities associated with the buoyancy circulation in a convective basin.

High-resolution regional simulations with GCMs allow a better understanding the mechanisms responsible for the generation of eddies in the Labrador Sea. Instability of the West Greenland Current near Cape Desolation, where the bottom topography exhibits a sharp discontinuity, generates anticyclonic eddies that carry light, warm Irminger Current water to the interior of the Labrador Sea (Eden and Böning, 2002; Katsman *et al.*, 2004). This instability seems to be due to both barotropic (Eden and Böning, 2002), baroclinic (Bracco and Pedlosky, 2003; Bracco *et al.*, 2008) and mixed instability (Katsman *et al.*, 2004). In (2), only the baroclinic instability is reproduced. A coarse parameterization of barotropic instability could be introduced in the model by using the same parameterization with the barotropic boundary current instead of the baroclinic boundary current. If this were the case, and given the parameters utilized in this study, this would only increase the turbulent heat fluxes by a factor 2, which would not significantly affect the results.

b. Dense water formation in the boundary current

In this idealized model of a convective basin, eddies are essential as they connect the region where dense water is formed to the boundary current. After convection occurs in the

basin interior, it takes a couple years before all the newly formed dense water is "flushed out"[5] and the basin reaches steady state again. This memory of the basin interior results from the relatively slow eddy transfer of the newly formed dense water from the interior of the basin to the surrounding boundary current, which finally damps the influence of changes in dense water formation on dense water transport by the DWBC. Observations show that convection takes place not only in the center of the Labrador Sea, but also in the boundary current (Pickart *et al.*, 1997; Cuny *et al.*, 2005), which is not taken into account in this study. In the latter case, newly formed dense water would directly contribute to dense water export, as suggested by hindcast simulations (Deshayes *et al.*, 2007). Hence the interannual variability of dense water transport by the DWBC could be directly influenced, i.e., with no integrating mechanism, by changes in dense water formation within the boundary current. A recent study based on observations at depth in the Labrador Sea with autonomous floats suggests that the fluctuations in the formation of Labrador Sea water within the DWBC and the fluctuations in lateral eddy fluxes between the interior Labrador Sea and the DWBC contribute to the same order of magnitude to the interannual variability of dense water export (Palter *et al.*, 2008). Nevertheless, it is important to note that the latter study is based on observations from 1996 to 2002, when atmospheric forcing was weak and the rate of dense water formation in the interior Labrador Sea among the smallest during the last 50 yr (Deshayes *et al.*, 2007).

c. Variability in h_0

Repeated observations of the hydrography in the West Greenland Current suggest interannual variability in the thickness of warm water in the West Greenland Current (Myers *et al.*, 2007), hence in h_0. In this paper, we develop the model taking into account changes in v_w and assuming that h_0 is constant. Hence we do not discuss the model response to changes in h_0. Nevertheless, analytical developments of the model allow a discussion of how the model results depend on h_0, in particular the fact that dense water formation is hardly affected by barotropic boundary current forcing. There is a minimum value for h_0 so that hypothesis (9) is valid (for the chosen parameters and forcings, h_0 must be larger than 147 m). Hence if h_0 tends to zero, i.e., warm water only is advected at the inflow, nonlinearities become important and our results are not valid any more. When the model is in the linear regime, the memory time scale for the basin interior depends on h_0 via the baroclinic velocity at the inflow (Eq. 12): the more warm water at the inflow, the faster the adjustment to fluctuations in the surface buoyancy fluxes.

d. Forcing time series

Observations of atmospheric conditions during convection suggest that large wind-stress is associated with larger buoyancy fluxes (e.g., Renfrew *et al.*, 2002). In the forcing time

5. Note that there is no net mass flux between the basin interior and the boundary current: eddies are responsible for lateral turbulent exchanges of buoyancy between the two regions that leads to diapycnal mixing in the boundary current.

series used in this study, though, fluctuations of surface buoyancy fluxes and wind-driven barotropic boundary current are not correlated on the interannual time scale. Indeed, the adjustment of the subpolar gyre barotropic circulation to wind forcing is affected by the presence of stratification at depth and topographic slopes, and takes a couple years as suggested by hindcast simulations (Deshayes and Frankignoul, 2008). Because the mechanisms of adjustment remain unclear, we decided to use v_w from a hindcast simulation rather than using an index of wind forcing directly, and created a time series of interannual fluctuations in the wind-driven barotropic boundary current that is not correlated with fluctuations in the surface buoyancy forcing. Note that because the model is linear when applied to the Labrador Sea, the results would be the same if fluctuations in the forcings were correlated, or if the power spectrum density of the forcings depended on frequency, although they would not be so visible.

e. Transition to nonlinear regime

Our model simulations for the Labrador Sea suggest a "clean" separation between the impact of the buoyancy forcing and that of the wind-driven barotropic boundary current forcing: the former mostly influences dense water formation in the interior of the basin, while the latter drives most of the fluctuations in dense water transport at the exit of the basin. It is important to discuss when this clean separation breaks down.

That dense water formation in the interior of the basin is hardly affected by the barotropic boundary current forcing, comes from the fact that the model is in the linear regime when applied to the Labrador Sea. Nonlinearities of the model cannot be neglected if γ (8) is of order (or larger than) 1. The first term of γ is smaller than 1 for all parameters and forcings, except if $h_0 > H$ (which is highly unrealistic for any convective basin), and it is $\mathcal{O}(1)$ when $v_w > 0$, whatever the parameters. The second term of γ, $\epsilon = cP/L$, is a measure of the eddy efficiency at transferring heat from the boundary current to the interior of the basin. As discussed above, if $\epsilon > 10$ (for the chosen set of parameters, $\epsilon = 0.43$), $\gamma > 1$ (Fig. 12) then eddies would be efficient enough so that wind-driven barotropic boundary current forcing significantly affects dense water formation in the interior of the basin.

The second hypothesis for neglecting nonlinearities, $\frac{AQ(t)}{g'Lv_w(t)h_0} << 1$ reads as the rate of buoyancy-driven dense water formation in the basin interior being much smaller than the wind-driven inflowing transport of dense water. If the inflowing transport of dense water were five times smaller (or surface buoyancy fluxes were five times larger), nonlinearities would be important (see also Straneo, 2006b) hence dense water formation in the interior of the basin would be significantly affected by the barotropic boundary current forcing.

Finally, the spectral shape of dense water transport at the exit of the basin depends on both buoyancy and wind-driven barotropic boundary current forcings (14). However, for the chosen forcing time series, fluctuations in the inflowing transport of dense water are larger than fluctuations in the rate of buoyancy-driven dense water formation in the interior of the basin ($r' = 0.61$ in experiment LABSEA). If r' where twice as large as

in experiment LABSEA, interranual fluctuations in dense water export would be more sensitive to buoyancy forcing.

f. Climatic implications of our results

When applying the model to the Labrador Sea case, the dense water transport at the exit of the convective basin T_P is interpreted as the transport of dense water in the DWBC in the southern Labrador Sea[6]. Further downstream, at midlatitude, the DWBC represents the deep limb of the MOC, and the associated transport of dense water is often used to estimate the intensity of the MOC. As a result, it is tempting to interpret the variability of T_P in our simple model as the variability of the MOC. Nevertheless, contradictory arguments suggest caution when drawing such an interpretation. On the one hand, in hindcast simulations, the transport of dense water by the DWBC in the southern Labrador Sea (i.e., T_P in the model) correlates with the MOC on interannual to decadal timescales (Böning *et al.*, 2006; Deshayes and Frankignoul, 2008). On the other hand, mid-depth floats released in the DWBC in the southern Labrador Sea are surprisingly reluctant to cross the North Atlantic Current and enter the subtropics, and rather recirculate around the subpolar gyre (Schott *et al.*, 2004; Haine *et al.*, 2008). The inconsistency is partly released by the modeling study of Getzlaff *et al.* (2006), who suggest that the float behavior (isobaric trajectories plus surfacing) is in part responsible for the unexpected float trajectories. However, they also suggest that only 10% of the water masses forming the DWBC in the southern Labrador Sea were transported by the DWBC downstream at midlatitude. Finally, as our simple model does not reproduce the splitting of the dense water masses that exit the convective basin into those that recirculate at high latitude and those that are actually exported to mid-latitudes, and considering the complexity of this mechanism and its potential impact on the MOC variability, variability in T_P in our simple model should be interpreted as variability of the DWBC in the southern Labrador Sea only.

The main result of the paper is that interannual fluctuations in the dense water transport in the southern Labrador Sea are dominated by changes in the wind-driven barotropic circulation, and are hardly affected by changes in dense water formation in the interior Labrador Sea. This is not inconsistent with observations of anomalous pulses of newly formed Labrador Sea Water (hereafter LSW) in the subtropical DWBC a decade or so after high convective years (Molinari *et al.*, 1998; Smethie and Fine, 2001). Indeed, T_P in the model represents the transport of water masses in LSW density class, a mixture of recently formed dense water and dense water that recirculated around the subpolar gyre and entered the basin at the boundary current inflow via T_0. In the model, fluctuations in the outflowing transport of *recently* formed dense water are strongly affected by changes in the surface buoyancy forcing but hardly affected by changes in the barotropic boundary current

6. It is important to mention again that this simple model does not represent water masses denser than those produced in the Labrador Sea, which do not seem to contribute to interannual to decadal variability of the DWBC (Beismann and Barnier, 2004). In general in this paper, dense water designates water masses of the same density as Labrador Sea Water (LSW) formed in the interior Labrador Sea.

forcing (not shown). Besides, the anomalous pulse of LSW observed at midlatitude after high convective years may be due to (1) deep convection in the boundary currents of the Labrador Sea, which is not reproduced in the model, and (2) so much LSW being formed in the interior of the Labrador Sea and recirculating in the interior subpolar gyre that it finally leads to an increase in h_0. As discussed above, in this paper, we assume that h_0 is constant, hence we do not comment on the model response to a change in h_0. Nevertheless, note that the outflowing transport of dense water in the model depends on h_0 via T_0 (Eq. 13): the more dense water at the inflow of the Labrador Sea, the larger the outflowing transport of dense water in the southern Labrador Sea.

7. Summary

This work is based on the earlier studies of Spall (2004) and Straneo (2006b) that contributed to understanding the dynamics of a convective basin, in particular the role of eddies. Here we address the question of the interaction between surface buoyancy forcing that induces dense water formation in the interior of the basin, and wind forcing as represented by a barotropic current around the basin. Moreover, while the two studies above focus on the steady state circulation and its seasonal fluctuations, this study considers the variability of the formation and export of dense water due to seasonal to decadal variability in both forcings.

The model is developed for any convective basin but the parameters and forcings are chosen to represent the Labrador Sea case. We first show that changes in dense water formation are influenced by changes in surface buoyancy forcing, but are not sensitive to (wind-driven) changes in the barotropic boundary current. Specifically, the interior tends to integrate the fluctuations in surface buoyancy forcing with a decadal time scale, that is set by eddies. Hence the interior of the basin exhibits most variability at decadal and longer periods, and reduced variability at higher frequency with respect to the variability of the surface buoyancy forcing. That dense water volume in the interior of the Labrador Sea integrates the surface buoyancy forcing is not surprising and consistent with observations of potential energy anomalies in the interior of the basin from 1950 to 1997 (Curry and McCartney, 2001). However, that small spatial scale, short-lived eddies may be responsible for a predominant decadal variability in the Labrador Sea is a major insight of this study.

The integrating mechanism, which can be seen as a memory of the interior Labrador Sea, does not appear in the dense water export whose variability is instead dominated by changes in the barotropic boundary current forcing via the inflowing transport of dense water. Indeed, variations in the barotropic boundary current forcing induce an increase in the variability of dense water export on interannual to decadal time scales, compared to variability of dense water export induced by changes in the surface buoyancy forcing alone. This suggests that interannual variability of dense water transport by the DWBC at the ouflow of the Labrador Sea is primarily induced by fluctuations in the wind-driven North Atlantic subpolar gyre. Noteworthy, variability in the diapycnal mixing within the boundary current, i.e., variability

in the PHT in this simple model, has maximum variance at decadal and longer periods and reduced variance at higher frequencies, similarly to variability of dense water formation.

Our results suggest caution when estimating variability of the MOC from observations of the DWBC in the subpolar gyre. Indeed, interannual variability of the transport of dense water by the DWBC at the outflow of the Labrador Sea is not related to changes in dense water formation, but reflects variability in the boundary currents of the subpolar gyre, which are primarily forced by the wind. On the other hand, in our simple model, variability in the amount of dense water in the interior of the Labrador Sea has the same characteristics as the PHT, which is actually the oceanic variable of climatic interest. This suggests that we should monitor the fluctuations in the amount of dense water in the subpolar North Atlantic.

Acknowledgments. Support for JD from the NOAA Office of Hydrologic Development through a scientific appointment administered by UCAR is gratefully acknowledged. Support for FS was provided by NSF grant OCE−0525929. Support for MAS was provided by NSF grant OCE−0423975.

APPENDIX

Linearization of the model

There are two nonlinear terms in the model equations: (i) the divergence term in the continuity equation for the lower layer of the boundary current (7) and (ii) the eddy fluxes parameterization in (6) and (7). Changes in the dense water thickness in the boundary current are written as anomalies from the inflow conditions:

$$h(t,l) = h_0 + h'(t,l). \tag{15}$$

Introducing (15) in (5), we derive an expression for the changes in lower layer velocity along the perimeter of the basin:

$$\frac{\partial v(t,l)}{\partial l} = \left(v^* \frac{D(t) + H - 2h_0}{H^2} - v^* \frac{2h'(t,l)}{H^2} \right) \frac{\partial h'(t,l)}{\partial l}. \tag{16}$$

If the changes in dense layer thickness in the boundary current are small compared to the inflow condition, i.e. $h'(t,l) << h_0$ (Hypothesis #1), $\frac{\partial}{\partial l}\{v(t,l)h(t,l)\}$ linearizes to $(v_w + h_0 v^* \frac{D(t)+H-2h_0}{H^2}) \frac{\partial h'(t,l)}{\partial l}$. If the changes in the baroclinic velocity in the boundary current are small compared to the inflow, i.e. $h'(t,l) << D(t) - h_0$ (Hypothesis #2), then $(D(t) - h(t,l))^2$ linearizes to $(D(t) - h_0)(D(t) - h_0 - 2h'(t,l))$.

Assuming that these two hypotheses are true hence that the two linearizations are valid, (7) simplifies in

$$\left(v_w + h_0 v^* \frac{D(t) + H - 2h_0}{H^2} \right)^{-1} \frac{\partial h'(t,l)}{\partial t} + \frac{\partial h'(t,l)}{\partial l} = \frac{\gamma}{P}(D(t) - h_0 - 2h'(t,l)) \tag{17}$$

$$\text{with} \qquad \gamma = \frac{v^*(D(t) - h_0)/H}{v_w + h_0 v^*(D(t) + H - 2h_0)/H^2} \times \frac{cP}{L}$$

Consider the case when $D(t)$ has reached a steady state D_{eq}. The boundary current adjusts to the interior within a time scale $\tau = \mathcal{O}(P/(2\gamma v_w))$, which is of the order of 18 months for the chosen parameters and forcings.

In the linear case, on time scales longer than $(P/(2\gamma v_w))$, the first term in the left hand side of (17) can be neglected and anomalies in the dense water thickness in the boundary current simply verifies

$$\frac{\partial h'(t,l)}{\partial l} = \frac{\gamma}{P}(D(t) - h_0 - 2h'(t,l))$$

which solves into

$$h'(t,l) = \frac{1}{2}(D(t) - h_0)\left(1 - e^{\frac{-2\gamma l}{P}}\right).$$

Hypotheses #1 and #2, which are necessary to ensure that non-linearities can be neglected to first order, depend on the model solution. Hence they cannot be used to determine a priori (ie for a given set of parameters and forcings) whether non-linearities will play a major role. Still, according to (10), Hypothesis #2 is verified as long as $\gamma << 1$, hence (8). It is not as straightforward to relate Hypothesis #1 to a non-dimensional criterion on the model forcings and parameters. Hereafter we only consider the case when $\forall t$, $h_0 \leq D(t)$, assuming that 1) the interior of the basin is the region where most dense water is formed and 2) the thickness of the recirculating dense water from the interior to the inflowing boundary current remains smaller than that in the interior of the basin. As a result, $\frac{\partial h'(t,l)}{\partial l} \geq 0$ hence $h'(t,l) \leq h'(t,P)$ and $D(t) \leq (h_0 + h'(t,l))$. According to (16), $\frac{\partial v(t,l)}{\partial l} > 0$, hence $v(t,l) \leq v(t,P)$. Dense water export is maximum if all the newly formed dense water is flushed out of the basin, which writes $v(t,P) \times (h_0 + h'(t,P)) \leq \frac{AQ}{g'L} + v_w \times h_0$. At the basin outflow, the smaller the increase in lower layer velocity, the larger the increase in lower layer thickness, which induces $h'(t,P) \leq \frac{AQ}{g'Lv_w}$. As a result, $\frac{AQ}{g'Lv_w h_0} << 1$ is a sufficient (though not necessary) criterion to ensure Hypothesis #1 is verified, hence (9).

REFERENCES

Beismann J.-O. and B. Barnier. 2004. Variability of the meridional overturning circulation of the North Atlantic: Sensitivity to overflows of dense water masses. Ocean Dyn., *54*, 92–106.

Böning C. W., M. Scheinert, J. Dengg, A. Biastoch and A. Funk. 2006. Decadal variability of subpolar gyre transport and its reverberation in the North Atlantic overturning. Geophys. Res. Lett., *33*, doi: 10.1029/2006GL026906.

Bracco A. and J. Pedlosky. 2003. Vortex generation by topography in locally unstable baroclinic flows. J. Phys. Oceanogr., *33*, 207–219.

Bracco A., J. Pedlosky and R. S. Pickart. 2008. Eddy formation near the west coast of Greenland. J. Phys. Oceanogr., *38*, 1992–2002.

Chanut J., B. Barnier, W. Large, L. Debreu, T. Penduff and J.-M. Molines. 2008. Mesoscale eddies in the Labrador Sea and their contribution to convection and re-stratification. J. Phys. Oceanogr., *38*, 1617–1643.

Cuny J., P. B. Rhines and J. R. N. Lazier. 2005. Convection above the Labrador continental slope. J. Phys. Oceanogr., *35*, 489–511.

Cuny J., P. B. Rhines, P. P. Niiler and S. Bacon. 2002. Labrador Sea boundary currents and the fate of the Irminger Sea Water. J. Phys. Oceanogr., *32*, 627–647.

Curry R. G. and M. S. McCartney. 2001. Ocean Gyre circulation changes associated with the North Atlantic Oscillation. J. Phys. Oceanogr., *31*, 3374–3400.

Deshayes J. and C. Frankignoul. 2005. Spectral characteristics of the response of the meridional overturning circulation to deep water formation. J. Phys. Oceanogr., *35*, 1813–1825.

—— 2008. Simulated variability of the circulation in the North Atlantic from 1953 to 2003. J. Climate, *21*, 4919–4933.

Deshayes J., C. Frankignoul and H. Drange. 2007. Formation and export of deep water in the Labrador and Irminger Seas in a GCM. Deep Sea Res. I, *54*, 510–532.

Eden C. and C. W. Böning. 2002. Sources of eddy kinetic energy in the Labrador Sea. J. Phys. Oceanogr., *32*, 3346–3363.

Eden C. and J. Willebrand. 2001. Mechanism of interannual to decadal variability of the North Atlantic circulation. J. Climate, *14*, 2266–2280.

Falina A., A. Sarafanov and A. Sokov. 2007. Variability and renewal of Labrador Sea Water in the Irminger Basin in 1991–2004. J. Geophys. Res., *112*, doi: 10.1029/2005JC003348.

Getzlaff, K., C. W. Böning and J. Dengg. 2006. Lagrangian perspectives of deep water export from the subpolar North Atlantic. Geophys. Res. Lett., *33*, doi: 10.1029/2006GL026470.

Haine T., C. Böning, P. Brandt, J. Fischer, A. Funk, D. Kieke, E. Kvalebert, M. Rhein and M. Visbeck. 2008. North Atlantic deep water formation in the Labrador Sea, recirculation through the subpolar gyre, and discharge to the subtropics, *in* Arctic-Subarctic Ocean Fluxes, R. R. Dickson *et al*., eds., 652–701.

Hall M. M. and D. J. Torres. 2008. Absolute velocity in the Labrador Sea: ADCP Observations along AR7W. Ocean Sciences Meeting 2008, *poster*.

Hawkins E. and R. Sutton. 2007. Variability of the Atlantic thermohaline circulation described by three-dimensional empirical orthogonal functions. Clim. Dyn., *29*, 745–762.

Jayne S. R. and J. Marotzke. 2001. The dynamics of ocean heat transport variability. Rev. Geophys., *39*, 385–411.

Johnson H. L., D. P. Marshall and D. A. J. Sproson. 2007. Reconciling theories of a mechanically driven meridional overturning circulation with thermohaline forcing and multiple equilibria. Clim. Dyn., *29*, 821–836.

Kalnay, E. *et al.* 1996. The NCEP/NCAR 40-Year Reanalysis Project. B. A. M. S., *77*, 437–471.

Katsman C. A., M. A. Spall and R. S. Pickart. 2004. Boundary current eddies and their role in the restratification of the Labrador Sea. J. Phys. Oceanogr., *34*, 1967–1983.

Lavender K. L., R. E. Davis and W. B. Owens. 2000. Mid-depth recirculation observed in the interior Labrador and Irminger seas by direct velocity measurements. Nature, *407*, 66–69.

Lilly J. M., P. B. Rhines, F. A. Schott, K. L. Lavender, J. R. N. Lazier, U. Send and E. D'Asaro. 2003. Observations of the Labrador Sea eddy field. Prog. Oceanogr., *59*, 75–176.

Marshall J. and F. A. Schott. 1999. Open ocean convection: observations, theory and models. Rev. Geophys., *37*, 1–64.

McMynowski D. G. and E. Tziperman. 2006. Two-way feedback interaction between the thermohaline and wind-driven circulations. J. Phys. Oceanogr., *36*, 914–929.

Mignot J., A. Ganopolski and A. Levermann. 2007. Atlantic subsurface temperatures: response to a shutdown of the overturning circulation and consequences for its recovery. J. Climate, *20*, 4884–4898.

Molinari R. L., R. A. Fine, W. D. Wilson, R. G. Curry, J. Abell and M. S. McCartney. 1998. The arrival of recently formed Labrador Sea water in the deep western boundary current at 26.5°N. Geophys. Res. Lett., *25*, 2249–2252.

Myers P. G., N. Kulan and M. H. Ribergaard. 2007. Irminger Water variability in the West Greenland Current. Geophys. Res. Lett., *34*, doi: 10.1029/2007GL030419.

Palter J. B., M. S. Lozier and K. L. Lavender. 2008. How does Labrador Sea Water enter the Deep Western Boundary Current? J. Phys. Oceanogr., *38*, 968–983.

Pickart R. S. and M. A. Spall. 2007. Impact of Labrador Sea convection on the North Atlantic meridional overturning circulation. J. Phys. Oceanogr., *37*, 2207–2227.

Pickart R. S., M. A. Spall and J. R. N. Lazier. 1997. Mid-depth ventilation in the western boundary current system of the subpolar gyre. Deep Sea Res. I, *44*, 1025–1054.

Pickart R. S., M. A. Spall and M. H. Ribergaard. 2003. Deep convection in the Irminger Sea forced by the Greenland tip jet. Nature, *424*, 152–156.

Pohlmann H., F. Sienz and M. Latif. 2006. Influence of the multidecadal Atlantic meridional overturning circulation variability on European climate. J. Climate, *19*, 6062–6067.

Renfrew I. A., G. W. K. Moore, P. S. Guest and K. Bumke. 2002. A comparison of surface layer and surface turbulent flux observations over the Labrador Sea with ECMWF analyses and NCEP reanalyses. J. Phys. Oceanogr., *32*, 383–400.

Schott F. A., R. Zantopp, L. Stramma, M. Dengler, J. Fischer and M. Wibaux. 2004. Circulation and deep water export at the western exit of the subpolar North Atlantic. J. Phys. Oceanogr., *34*, 817–843.

Smethie W. M. and R. A. Fine. 2001. Rates of North Atlantic deep water formation calculated from chlorofluorocarbon inventories. Deep-Sea Res. I, *48*, 189–215.

Spall M. A. 2004. Boundary currents and water mass transformation in marginal seas. J. Phys. Oceanogr., *34*, 1197–1213.

Spall M. A. and D.C. Chapman. 1998. On the efficiency of baroclinic eddy heat transport across narrow fronts. J. Phys. Oceanogr., *28*, 2275–2287.

Stouffer R. J., J. Yin, J. M. Gregory, K. W. Dixon, M. J. Spelman, W. Hurlin, A. J. Weaver, M. Eby, G. M. Flato, H. Hasumi, A. Hu, J. H. Jungclaus, I. V. Kamenkovich, A. Levermann, M. Montoya, S. Murakami, S. Nawrath, A. Oka, W. R. Peltier, D. Y. Robitaille, A. Sokolov, G. Vettoretti and S. L. Weber. 2006. Investigating the causes of the response of the thermohaline circulation to past and future climate changes. J. Climate, *19*, 1365–1387.

Straneo F. 2006a. Heat and freshwater transport through the central Labrador Sea. J. Phys. Oceanogr., *36*, 606–628.

—— 2006b. On the connection between dense water formation, overturning and poleward heat transport in a convective basin. J. Phys. Oceanogr., *36*, 1822–1840.

Talley L. D. 2003. Shallow, intermediate, and deep overturning components of the global heat budget. J. Phys. Oceanogr., *33*, 530–560.

Talley L. D. and M. S. McCartney. 1982. Distribution and circulation of Labrador Sea Water. J. Phys. Oceanogr., *12*, 1189–1204.

Trenberth K. E. and J. M. Caron. 2001. Estimates of meridional atmosphere and ocean heat transports. J. Climate, *14*, 3433–3443.

Vellinga M. and R. A. Wood. 2002. Global climatic impacts of a collapse of the Atlantic thermohaline circulation. Climatic Change, *54*, 251–267.

Visbeck M., J. Marshall, T. Haine and M. Spall. 1997. Specification of eddy transfer coefficients in coarse-resolution ocean circulation models. J. Phys. Oceanogr., *27*, 381–402.

Visbeck M., J. Marshall and H. Jones. 1996. Dynamics of isolated convective regions in the ocean. J. Phys. Oceanogr., *26*, 1721–1734.

Zhu X., K. Fraedrich and R. Blender. 2006. Variability regimes of simulated Atlantic MOC. Geophys. Res. Lett., *33*, doi: 10.1029/2006GL027291.

Received: *6 November, 2008*; revised: *9 July, 2009*.